Accepted 2000 April 20 for publication in The Astrophysical Journal
Preprint typeset using LaTeX style emulateapj v. 04/03/99

arXiv:astro-ph/0005032v1 2 May 2000

ORBITAL DYNAMICS OF CYGNUS X-3

M.M. Hanson[1], M.D. Still[2,4], R.P. Fender[3]
[1]Department of Physics, The University of Cincinnati, Cincinnati, OH 45221-0011
[2]NASA/Goddard Space Flight Center, Code 662, Greenbelt, MD, 20771
[3]Astronomical Institute 'Anton Pannekoek', University of Amsterdam, and Center for High Energy Astrophysics, Kruislaan 403, 1098 SJ, Amsterdam, The Netherlands
Accepted 2000 April 20 for publication in The Astrophysical Journal

ABSTRACT

Orbital-phased-resolved infrared spectra of Cygnus X-3 in outburst and quiescence, including tomographic analysis, are presented. We confirm the phasing of broad He II and N V lines in quiescence, such that maximum blue shift corresponds to the X-ray minimum at $\Phi = 0.00 \pm 0.04$. In outburst, double-peaked He I structures show a similar phasing with two significant differences: (a) although varying in relative strength, there is continuous line emission in blue and red peaks around the orbit, and (b) an absorption component, $\sim 1/4$ of an orbit out of phase with the emission features, is discerned. Doppler tomograms of the double-peaked profiles are consistent with a disk-wind geometry, rotating at velocities of 1000 km s^{-1}. Regrettably, the tomography algorithm will produce a similar ring structure from alternative line sources if contaminated by overlying P Cygni profiles. This is certainly the case in the strong 2.0587 μm He I line, leading to an ambiguous solution for the nature of double-peaked emission. The absorption feature, detected 1/4 of an orbit out of phase with the emission features, is consistent with an origin in the He star wind and yields for the first time a plausible radial velocity curve for the system. We directly derive the mass function of the system, 0.027 $M_\odot$. If we assume a neutron star accretor and adopt a high orbital inclination, $i > 60^\circ$, we obtain a mass range for the He star of $5\ M_\odot \lesssim M_{WR} \lesssim 11\ M_\odot$. Alternatively if the compact object is a black hole, we estimate $M_{BH} \lesssim 10\ M_\odot$. We discuss the implications of these masses for the nature and size of the binary system.

Subject headings: binaries : close – stars : individual : Cygnus X-3 – circumstellar matter – infrared : stars

1. INTRODUCTION

First discovered in the pioneering X-ray surveys of the 1960s, Cygnus X-3 (Cyg X-3) remains among the least understood of the long-standing X-ray sources known in the sky. In the early 1970s, it was discovered to show a flux modulation on a period of 4.8 hours, first in X-rays (Parsignault et al. 1972; Sanford & Hawkins 1972) and then also at near-infrared wavelengths (Becklin et al. 1973), which was assumed to be the orbital period of the binary system. Modulation of the light curve at this period is asymmetric and extremely similar in both X-ray and infrared bands (Mason, Cordova & White 1986), with the exception of irregular, rapid flaring superposed on the orbital modulation in the infrared (Mason et al. 1986; Fender et al. 1996). The period of this orbit was further shown to be rapidly increasing, with a time-scale of just 850,000 yrs (Kitamoto et al. 1995).

Van den Heuvel & De Loore (1973) made the prediction that the system was comprised of a compact object and a helium star, thus representing a remarkably rare, late evolutionary stage of a massive X-ray binary. Nearly 20 years later, persuasive evidence to support this prediction was found in near-infrared spectroscopic data presented by van Kerkwijk et al. (1992; 1996). They discovered strong, broad emission lines of neutral and ionized helium, combined with a marked lack of hydrogen features. These properties are reminiscent of massive, highly evolved stars known as Wolf-Rayet stars (Smith 1968). As such, Cyg X-3 represents one of the most unique binary systems in our Galaxy. Should the helium companion star become a supernova, as is generally predicted for Wolf-Rayet stars (however, cf. Conti 1996), it could evolve into a double compact object binary system, such as the Hulse-Taylor pulsar, PSR 1913+16 (Hulse & Taylor 1975; Burrows & Woosley 1986). In addition, Cyg X-3 is one of the most luminous sources of radio jets in our Galaxy, displaying repeated ejections at (probably) relativistic velocities (e.g. Schalinski et al. 1998).

While much data have been gathered on the system through X-ray, near-infrared and radio observations, the most fundamental properties of the Cyg X-3 system have been difficult to constrain. This is a consequence of line emission found to be dominated by a non-axisymmetric wind component rather than one or both of the stellar objects. Furthermore, the wind features are generally weak, very broad and at times heavily blended, making line identification difficult or impossible. Consequently stellar masses have not been measured from binary motion. There exist plausible arguments for both a high (Schmutz, Geballe & Schild 1996) and low (Mitra 1996, 1998) mass companion star, which has inevitable consequences for the state of the compact object, be it a neutron star or a black hole. As the only known Wolf-Rayet + compact object binary and (probably) the shortest-period high-mass X-ray binary, accurate constraints on the mass and dimensions of the Cyg X-3 system are crucial for our understanding of many aspects of massive binary evolution.

In a previous paper (Fender, Hanson, & Pooley 1999,

[4]Also Universities Space Research Association

hereafter FHP99), we found a dramatic spectral change during an outburst of the system. Though the lines suffer from serious blending, it would appear that during outburst the spectrum of the system evolves from showing high-excitation single-peaked emission lines to one dominated by low-excitation double-peaked profiles. In this current paper we present a first analysis of these data in order to map the velocity field of the line-emitting regions.

2. OBSERVATIONS

We have recently completed a monitoring program of the Cyg X-3 system spanning 18 months. Our observations are based on broadband radio observations at 15 GHz combined with the Rossi XTE All-Sky Monitor program (FHP99). During this monitoring program we obtained the best near-infrared spectroscopy of the system, intermittently throughout the 18 months. These data, comprising over 100 individual spectra taken of Cyg X-3, were obtained over four different observing campaigns between May 1996 and October 1997. The data are available through the CDS archive website (see FHP99).

The near-infrared spectroscopic data used in this analysis are presented and fully described in FHP99. Observations were made using the Steward Observatory's infrared spectrometer, FSpec (Williams, et al. 1993) on the Multiple Mirror Telescope prior to the recent upgrade to a single mirror. The spectra have an effective resolution of R $\approx$ 1200 at 2.12 μm, and a spectral coverage from 2.02 μm to 2.22 μm. Our analysis in this paper is based on epochs A, C and D, as defined by FHP99. The Cyg X-3 system was in quiescent-, outburst- and post-outburst mode, respectively, during these three epochs. Figure 1 displays spectra taken from each epoch in order to show the main spectral features present during these three epochs. In quiescence the K-band is dominated by broad, weak He II and N V emission; in outburst strong twin-peaked He I emission dominates; for a detailed discussion see FHP99.

3. ANALYSIS

Because of the night-to-night variations of the emission line profiles observed during the outburst phase (see FHP99), it was important to obtain full orbital coverage on a single night for this analysis. We have time-resolved spectra providing full orbital sampling during two nights, 1996 June 2–3, when the system was in quiescence and 1997 June 19–20, when the system was in outburst. Despite the heavy blending, we were able to identify a few of the major features within the spectra using the laboratory transition lists of Morris et al. (1996).

3.1. *June 1996 Quiescent Spectra*

Trailed spectra from 1996 June are presented in the upper three panels of Fig 2. In each case, the continuum was removed by subtracting a 3-spline fit to nearby line-free wavelength regions and the data were recast into constant velocity bins of 121 km s^{-1}. Spectra were further mean-averaged into 10 orbital phase bins using the ephemeris of Kitamoto et al. (1995). Doppler tomograms were constructed from the trailed spectra using the Maximum Entropy Method (Marsh and Horne 1988), an approach preferred here over other mapping algorithms because it allows the mapping of blended lines such as the He II 2.1653,2.1891 μm doublet. It involves the transformation of velocity–phase information provided by the Doppler-broadened emission line profiles (V,Φ) to a velocity–velocity field (V_x,V_y) using:

$$f(V,\Phi) = \int\int I(V_x,V_y) \quad \times$$

$$g(V - \gamma + V_x \cos\Phi - V_y \sin\Phi)\ \mathrm{d}V_x\ \mathrm{d}V_y. \qquad (1)$$

The mapping results from a χ^2-iteration between model and a fit and entropy minimization (Skilling and Bryan 1984). f is the emission line intensity at velocity V and orbital phase Φ, I the emission distribution of the resulting map in velocity coordinates (V_x,V_y), γ the systemic velocity of the binary center of mass and $g(V)$ the local line profile. From the combination of Doppler-broadened line profiles and rotational profile variations over the orbit, the maps are reconstructions of line emission in the velocity field around the binary, where V_y is the velocity in the direction parallel to a line joining the two stellar centers and V_x is the velocity orthogonal to V_y in the plane of the orbit.

Any motion out of the orbital plane will not be recognized by the mapping and consequently Doppler tomograms are of most use in systems where line emission is confined to gas moving in a plane, such as distributed over an accretion disk or one of the stellar companions. If emission originates in a spherical wind the tomograms become difficult, if not impossible, to interpret with any confidence. Our motivation to apply tomographic mapping to the lines in Cyg X-3 is two-fold. First, in quiescence, the line emitting wind region is thought to be within the cone shadowed from the X-ray source by the companion star (van Kerkwijk et al. 1996). Motion in the cone is somewhat constrained to the orbital plane, although this assumption breaks down if the mass ratio $q = M_{\rm WR}/M_{\rm X}$ is too large. Secondly, FHP99 reveal that line emission profiles are double-peaked in outburst, suggesting that a disk or flattened, rotating wind may dominate profiles during these epochs, in which case Doppler tomography is well suited to these spectra.

The tomograms derived from the quiescent data of Fig 2 are shown in Fig 3. The reduced-χ^2 of these fits are listed in Table 1. For reference, the binary center of mass occurs at (V_x,V_y) = (0,0) km s^{-1}, The companion star center of mass corresponds to (V_x,V_y) = (0,$K_{\rm WR}$), where $K_{\rm WR}$ is the radial velocity of the Wolf-Rayet star, $K_{\rm WR} \geq 0$. The compact object center of mass occurs at (V_x,V_y) = (0,$-K_{\rm X}$) where $K_{\rm X}$ is the radial velocity semi-amplitude of the accreting star. The ratio $K_{\rm X}/K_{\rm WR} = q$, where q is the ratio of stellar masses. Rotating structure around the compact object or WR star will manifest itself as an annulus on the map centered on $K_{\rm X}$ or $K_{\rm WR}$, respectively. The lower panel of Fig 2 shows the model emission profiles produced from the tomographic fit in Fig 3.

The trailed spectra and Doppler tomograms indicate that the line emission in quiescence arises in a restricted region of velocity space. This is consistent with the van Kerkwijk model in which the line emission originates in a region of the stellar wind shadowed from ionizing X-rays by the He star. Note that the cool wind component and binary motion vectors are orthogonal: this results in the wind phasing and WR star phasing being separated

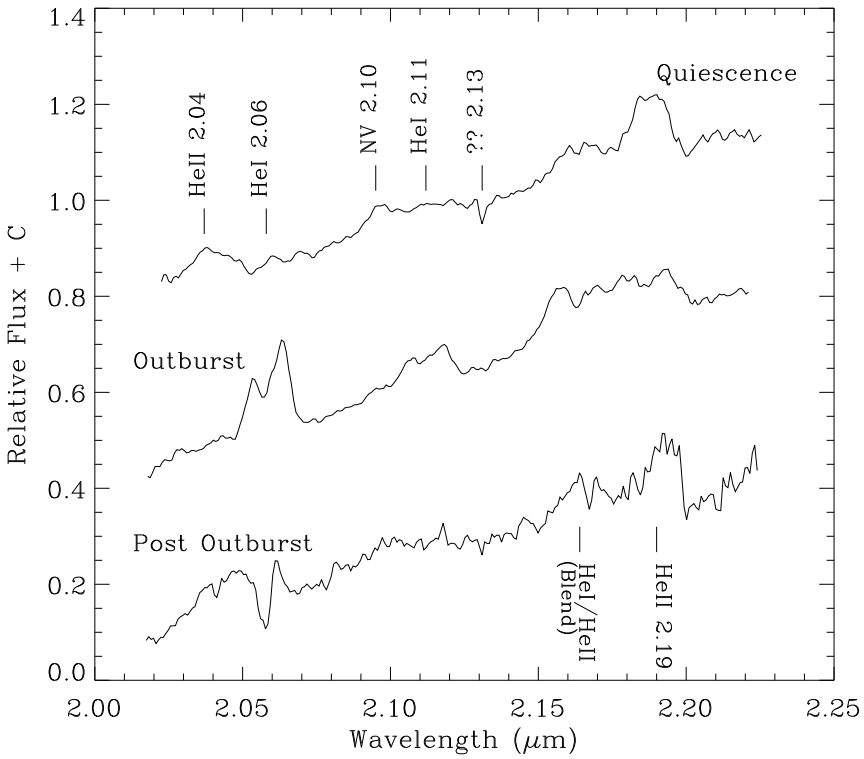

FIG. 1.— K-band spectra of Cyg X-3, each displayed with an arbitrary flux offset, 'C', for clarity. The quiescent spectrum shown at top was taken 6 June 1996 (epoch A, as defined by FHP99). The middle spectrum was taken 19 June 1997 (epoch C) during very extreme radio and X-ray flaring of the system. The bottom spectrum was taken 15 October 1997 (epoch D). During this time, small X-ray flaring was still occurring, but the system was now in 'post-outburst'.

TABLE 1
χ^2_ν FOR TOMOGRAPHIC FITS

Quiescence Line (μm)	χ^2_ν	Outburst Line (μm)	χ^2_ν
N V 2.1000	1.9	He I 2.0587	296.0
He II 2.0379	5.1	He I 2.1126	15.0
He II 2.1653/2.1891	5.2	He I 2.1623/2.1847	31.2

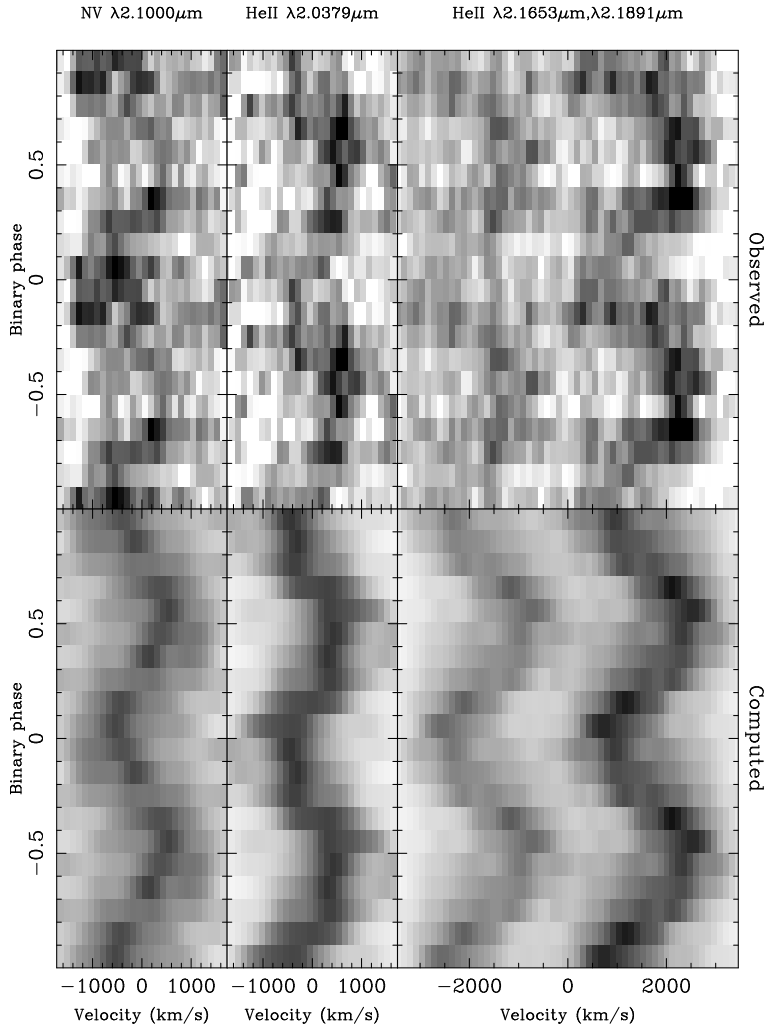

FIG. 2.— K-band trailed spectrograms representing full orbital phase coverage (4.8 hours) obtained on 2 June 1996. Spectral regions sampling the four strongest emission features of N V and He II are displayed. The data have been repeated over a second orbital cycle. These data were obtained while Cyg X-3 was in quiescence, as deemed by low radio and X-ray activity (see FHP99). The lower panel shows the model emission profiles produced from the tomographic fit in Fig 3. White to black corresponds to increasing emission intensity on individual linear scales. White coincides with the continuum level.

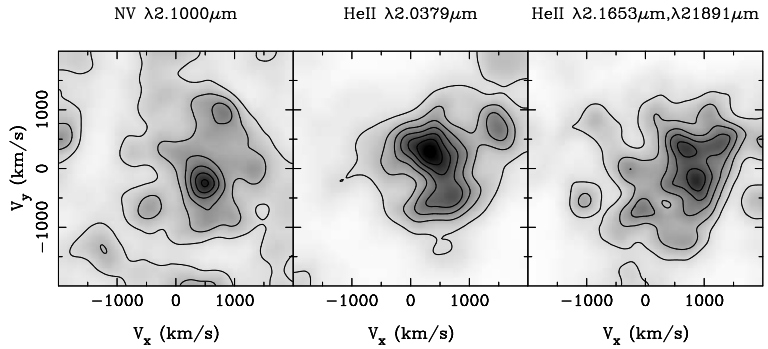

FIG. 3.— Doppler tomograms of the N V and He II lines during quiescence in June 1996. These are derived from computed fits of the data shown in upper panel of Figure 2. The intensity scales are as in Figure 2. The resulting fit from the tomographic modeling (described in eqn. 1) and their corresponding reduced-χ_2 are given in Table 2.

TABLE 2
LINE IDENTIFICATIONS AND MEASUREMENTS, JUNE 1996 QUIESCENT SPECTRA

		Gaussian Fit				Tomograms	
λ_{vac} (μm)	Line Identification	γ (km s^{-1})	K (km s^{-1})	FWHM (km s^{-1})	Φ	K (km s^{-1})	Φ
2.0379	He II (15-8)	+162±28	437±36	2959±201	−0.02±0.04	439±20	−0.135±0.05
2.100	N V (11-10)	−108±22	443±25	1928±322	+0.02±0.02	550±20	+0.08±0.04
2.1653	He II (14-8)	− 79±39	446±26	1618±124	+0.00±0.04	890±20	+0.03±0.02
2.1891	He II (10-7)	+152±20	577±56	2554±54	+0.16±0.02	"[a]	"

[a]Blended calculation

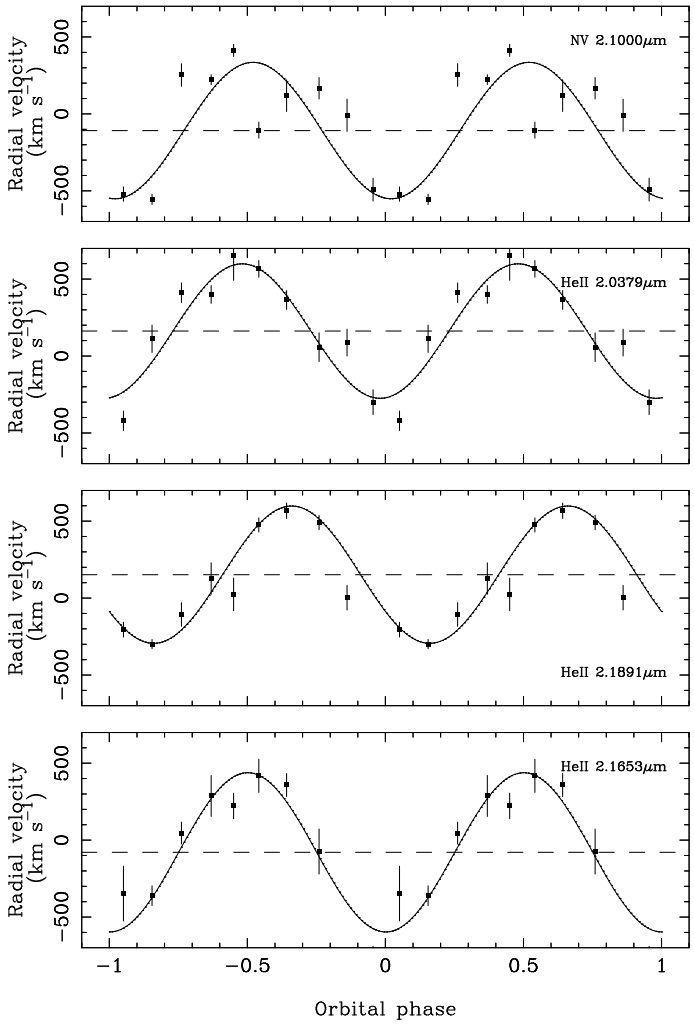

FIG. 4.— Radial velocity fits to the four emission features shown in Figure 2. Semi-amplitude peaks trace general wind velocities, which are also traced in the tomograms of Figure 3. The velocities determined from this and the tomographic analysis are given in Table 2.

90 degrees and the tomographic location of the emission occurring in a region offset approximately 90° from the tomographic location of the Wolf-Rayet star. Because of the moderate χ^2 of these fits the small scale structure is not significant.

Two-dimensional Gaussian fits to the tomograms provide a first-order estimate of both velocity, $K = \sqrt{V_x^2 + V_y^2}$, and phasing, $\Phi = \tan^{-1}(V_x/V_y)$, of the emitting gas and these are listed in Table 2. Uncertainties are not propagated through the mapping algorithm and therefore the errors are taken to be the size of a pixel element on the maps. Similar results are obtained by fitting one-dimensional, time-dependent Gaussian profiles to the raw data and this provides confidence in our tomographic fits. These further Gaussian fits are also presented in Table 2 and the resulting velocities plotted against orbital phase in Figure 4.

By taking a variance-weighted mean of the one-dimensional fits, the line forming region(s) have an average wind velocity of $K = 480 \pm 50$ km s^{-1}. This is consistent with the value measured by Schmutz et al. (1996). We do not detect any significant difference in K between the N V and the three He II lines in this measure. From the fits, an average full-width half-maximum (FWHM) value was determined for each of the four transitions, and is given in Table 2; if the lines are well represented by Gaussian profiles, these values imply a terminal wind velocity of at least 1500 km s^{-1} in the system, similar to that found by van Kerkwijk et al. (1996).

We have also more accurately determined the maximum of the blue-shifted wind features of He II and N V against the X-ray modulation. From a weighted-mean of the four measurements, the He II and N V features are at their maximum blue-shift when the X-ray intensity is at a minimum (e.g. Φ=0), with an error of 0.04 in orbital phase.

Note that there is no well-defined solution for the systemic velocity of the binary center of mass, γ (Eqn. 1), from the 1-dimensional fits in Table 2. This could be the result of turbulence within the wind (e.g., Lépine & Moffat 1999). Furthermore, the laboratory wavelength for the N V transition is not accurately known. γ can only be constrained to $|\gamma| \leq 200$ km s^{-1}, precluding us from making a distance estimate. This upper limit on the systemic velocity seems rather difficult to reconcile with the +800 km s^{-1} velocity field recently reported by Chandra observations of the system (Paerels et al. 2000).

3.2. *June 1997 Outburst Spectra*

The upper panel of Figure 5 shows the spectra taken during the June 1997 outburst. All lines seen have been attributed to He I, though exact line identifications for the $\lambda = 2.16 - 2.18$ μm region are difficult to make. There is likely some contamination from the 2.1891 μm He II feature normally seen during quiescence. Doppler tomograms, derived from the outburst spectra in Figure 5 are shown in Figure 6. Reduced-χ^2 of each fit are provided in Table 1. Finally, computed spectra, derived from the tomograms shown in Figure 6, are given in the lower panel of Figure 5.

The line profile behavior of the four He I lines appears at least marginally similar to that seen during quiescence: strong blue shifted emission at X-ray minimum and strong red shifted emission at X-ray maximum. However, the 2.0587 μm He I line in the outburst spectrum shows much stronger red-shifted emission at $\Phi = 0.5$ than the blue shifted emission at $\Phi = 0.0$ (Fig 5; see also Fig 4 of FHP99). Furthermore, in the region of the the 2.0587 μm He I line, a narrow, permanently blue-shifted absorption feature is seen, threaded through the background emission (Fig. 7).

The 2.1623 μm He I line appears almost double-peaked though, like the 2.0587 μm transition, the peak velocities are a bit asymmetric, showing strongest emission while at maximum red shift. Double-peaked emission may be evidence for rotating gas either in an accretion disk or a wind. However the stronger red peak also suggests these transitions may be contaminated by a P Cygni profile.

All three tomograms describe a ring structure similar to the tomographic signatures of an accretion disk (Fig. 6), consistent with rotational velocities on the order of 1000 km s^{-1}. Unfortunately the mapping algorithm assumes that all line components have a velocity modulating symmetrically about γ. P Cygni profiles break this assumption and it is possible that the entire ring structure in each map is the result of P Cygni absorption. P Cygni components will not be recreated in the computed spectra and this explains the large discrepancies between the real data and fits in Fig. 5. It is important that we consider only the real data in the upper panels when interpreting line behavior in this system. Note though that the fits are poor for the 2.0587 μm transition (Table 1) but improve for the other maps suggesting that any P Cygni contributions are reduced in these transitions. Consequently the case for a disk or rotating wind cannot be proven or ruled out in any of these transitions.

Fortunately, the sinusoidal absorption feature found in the 2.0587 μm spectral region is far less ambiguous, being clearly discerned over the entire temporal sequence of Figure 5 and 7. This continuous blue absorption feature was fit with a Gaussian to determine its velocity modulation over the orbital cycle. Without knowing the shape of the underlying emission profile, the fits to the absorption feature are dubious. However since the absorption feature is narrow, being just a few resolution elements across, any bias to the result should be small. The feature was found to oscillate with a semi-amplitude of $K = 109 \pm 13$ km s^{-1}. Most importantly, the phase of the velocity shifts, shown in Figure 8, are not like those seen in the N V and He II features during quiescence (Figure 2) or like the He I emission features during outburst, whose red and blue maxima occur at $\Phi = 0.5$ and 0.0 (Figure 4). Instead, the absorption shows red and blue maximum at phases, $\Phi = 0.18$ and 0.68 (with an error of ~ 0.02), relative to the orbital ephemeris of Kitamoto et al. (1995).

If $\Phi = 0$ corresponds to superior conjunction of the compact object in Cyg X-3, red and blue maxima of features associated with the mass donor He star should occur at $\Phi = 0.25$ and $\Phi = 0.75$, respectively. Thus the observed phasing of the absorption feature is approximately consistent with it tracing the motion of the He star. The impact of this result is explored further in Section 4.1. Fixing the phases of the maximum blue and red-shift to correspond with the binary phases $\Phi = 0.25$ and $\Phi = 0.75$ and refitting the radial velocity curves produces only a slightly poorer fit, $K = 100 \pm 14$ km s^{-1}, but with a consistent

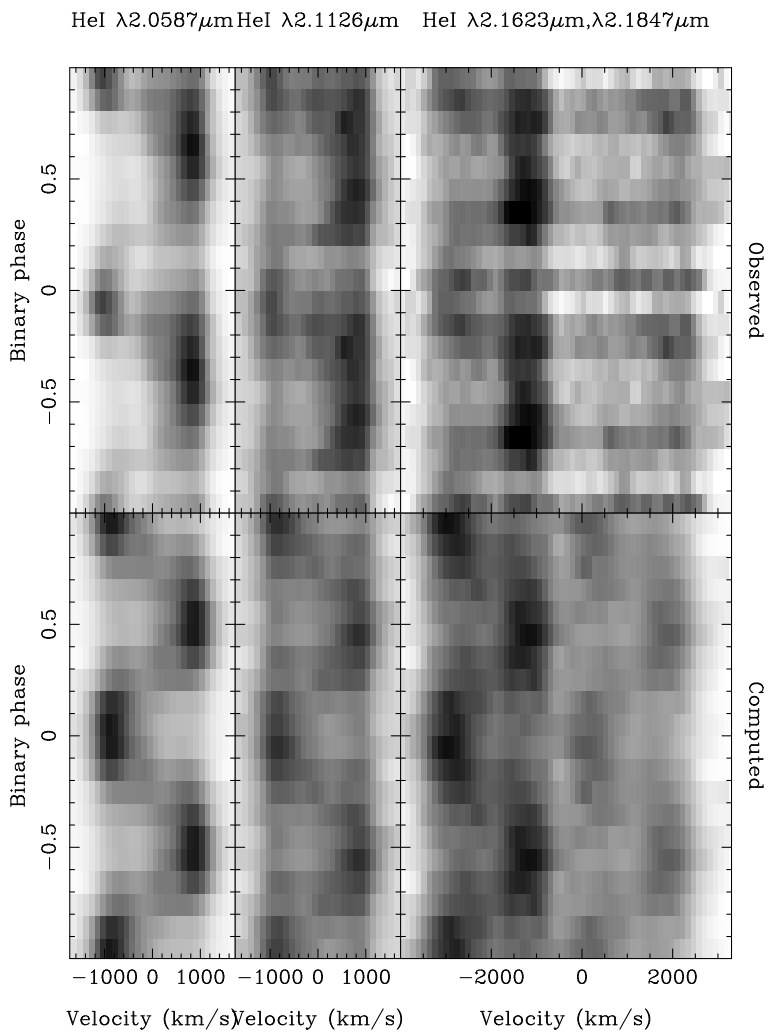

FIG. 5.— K-band trailed spectrograms representing full orbital phase coverage (4.8 hours) obtained on 19 June 1997. Spectral regions sampling the four strongest emission features of He I are displayed. The data have been repeated over a second orbital cycle. These data were obtained while Cyg X-3 was in outburst, as deemed by high radio and X-ray activity (see FHP99). The bottom panel shows the projected fits to the Doppler tomograms given in Figure 6. Similar to Figures 2 and 3, white to black corresponds to increasing emission intensity on individual linear scales, making white coincident with the continuum level.

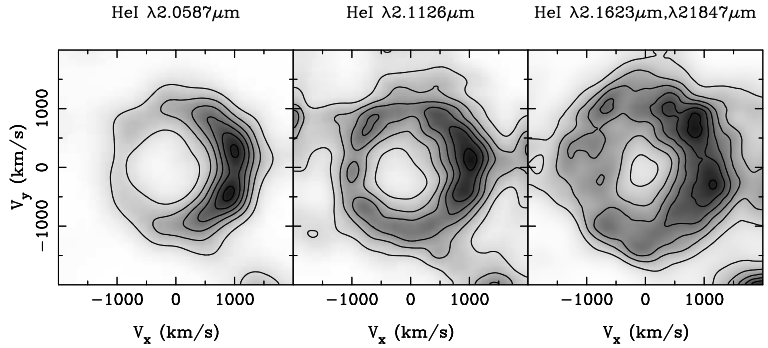

FIG. 6.— Doppler tomograms of the four He I lines during the June 1997 outburst, derived from the spectra given in the upper panel of Figure 5. The intensity scales are as in Figure 5.

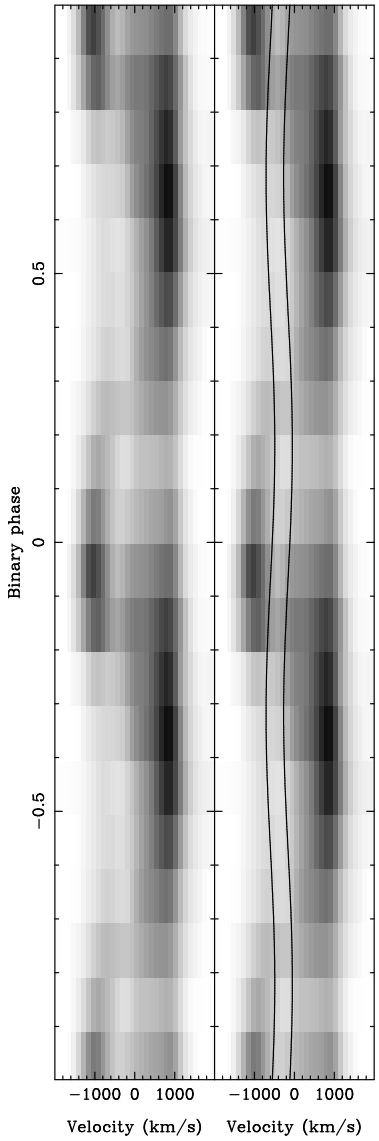

FIG. 7.— An expanded view of the full orbital phase coverage over a 4000 km s^{-1} velocity range centered on the He I 2.0587 μm line, as previously shown in Fig. 5. To the right is the same information, though marked with the location of the permanently blue-shift absorption feature. The absorption feature is seen as white against the broader underlying emission feature of the 2.0587 μm He I line.

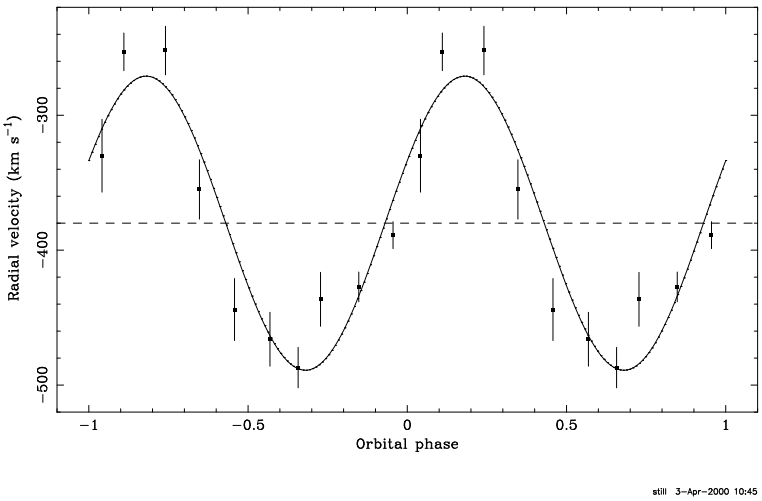

FIG. 8.— Gaussian fit to the absorption trough seen in the trailed, 2.0587 μm He I feature in Figure 7, as a function of X-ray phase. Parameters of the fit include: K = 109±13 km s^{-1}, with central velocity occurring at X-ray phase, Φ = -0.07±0.02. If Φ is set equal to 0.0, the corresponding value for K, 100±14 km s^{-1}, is near equally as good a solution. The values for K and Φ are independent of the exact identification of the spectral feature or features. The value for γ, shown in the above solution to be -380±10 km s^{-1}, assumes the feature is due to the He I 2.0587 μm line.

semi-amplitude.

4. DISCUSSION

4.1. *The He I 2.0587 μm transition*

Some very important differences in the formation of the He I transitions have been described. This has lead to very different line fluxes and quite possibly different line profiles seen in the numerous lines detected in the Cyg X-3 outburst spectrum. First, 2.0587 μm emission is produced by direct radiative recombination into the 2^1P state, or through recombinations at higher levels which then cascades down into the 2^1P state. This is not a problem in very dense extended winds, as the radiation field pumps electrons via the He I resonance lines into upper levels, leading to an enhancement of recombinations to the 2 ^1P level. However, once in this state, the atom has only a $\sim$ 1:1000 chance of decaying via the 2.0587 μm (2 ^1P − 2 ^1S) transition compared to the 584 Å (2 ^1P − 1 ^1S) resonant transition. Thus strong 2.0587 μm emission further requires a very high optical depth in the 584 Å line. There is a second equally important point about the He I 2.0587 μm line. Its lower level, 2 ^1S, is meta-stable and becomes increasingly overpopulated (relative to LTE). Frequently, a 2.0587 μm P Cygni profile is seen in hot, dense WR winds because in the outermost regions the absorption process becomes quickly favored due to the overpopulated lower level (Williams & Eenens 1989). Thus, the expected behavior of the 2.0587 μm line in an extended wind is for it to self-absorb readily, i.e., create a P Cygni feature. It is of interest to note that several months after the outburst in June 1997, the dominant feature in the spectrum of Cyg X-3 is the P Cygni profile occurring at 2.0587 μm (Fig 1, see also FHP99).

The remaining transitions, most specifically the $4s-3p$ triplet at 2.1126 μm (the singlet $4s-3p$ line at 2.1138 μm has about one third the flux of the combined emission from the triplet transition), are not directly coupled to a resonance transition. Their emission level is set only by the recombination rate of He^+. Furthermore, they are not predisposed to increased absorption in dense winds like the 2.0587 μm transition, since their lower states readily cascade to lower levels. These differences can give rise to rather different behaviors in the He I lines seen in our outburst spectra, and may possibly explain why the weak sinusoidal absorption feature seen threaded through outburst spectrum shown in Figure 5, is detected only in the 2.0587 μm He I line.

4.2. *Orbital dynamics from the He I 2.0587 μm absorption line*

Fortunately, an exact identification of the absorption feature seen in Figure 5 is not necessary for our purposes. While we feel confident the feature is due to He I 2.0587 μm given the arguments given above, even if the line is unknown, or due to an unresolved blend of features, we can still use its velocity signature given in K to measure the orbital dynamics of the Cyg X-3 system. As already noted, the phasing of the absorption feature seems consistent with a source which is distributed approximately isotropically around the star and hence should reflect the binary motion of the He star in the system. However, before continuing with that interpretation, we note that there have been alternative suggestions for the phasing of the system. For example Schmutz et al. (1996) propose that the He II and N V emission lines commonly observed in quiescence (Figure 2) track the motion of the He star (in which case X-ray minimum light would be occurring one quarter cycle before superior conjunction of the compact accretor). So it is clear that there is not a consensus about the interpretation of the phasing in the Cyg X-3 system. As a result we have investigated the implications of an origin for the absorption line to originate in material centered on the accretor and on the donor.

Dynamical solutions for the first case, that the absorption line in the material is centered on the accretor, are presented in Fig 9a. The solid curves show the mass solution assuming the compact object is a neutron star of M_x = 1.4 $M_\odot$. For this solution only, two solid curves are given to demonstrate the error range on the velocity

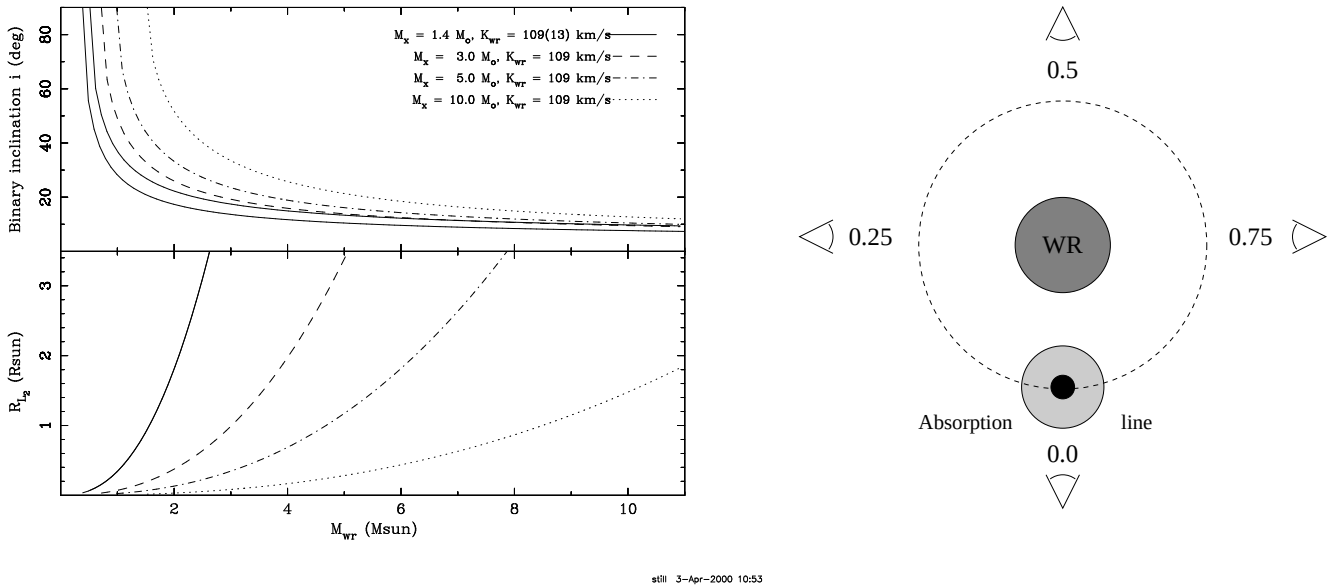

FIG. 9.— Orbital solutions assuming the motion traced in Figure 7 and 8 is centered on or associated with the motion of the compact object. On the left (9a) are shown orbital solutions for differing input mass of the companion (WR) object, displayed versus inclination angle of the binary system and Roche lobe radius. Solutions explored range from a compact object mass, $M_X = 1.4$ to 10 $M_\odot$. Two solid curves are given for the $M_X = 1.4$ $M_\odot$, solution, which illustrates the plus-minus error range on K. For any reasonable WR star mass, $M > 2$ $M_\odot$, only extremely low inclinations are possible. This is difficult to reconcile with the X-ray modulation. The orbital orientation implied by this interpretation is indicated in the panel to the right (9b). Such an interpretation is counterintuitive in the sense that it requires X-ray orbital minimum to occur when the X-ray source is nearest to the observer. All of these evidences disfavor the interpretation that the sinusoidal variations are centered on or associated with motion of the compact object.

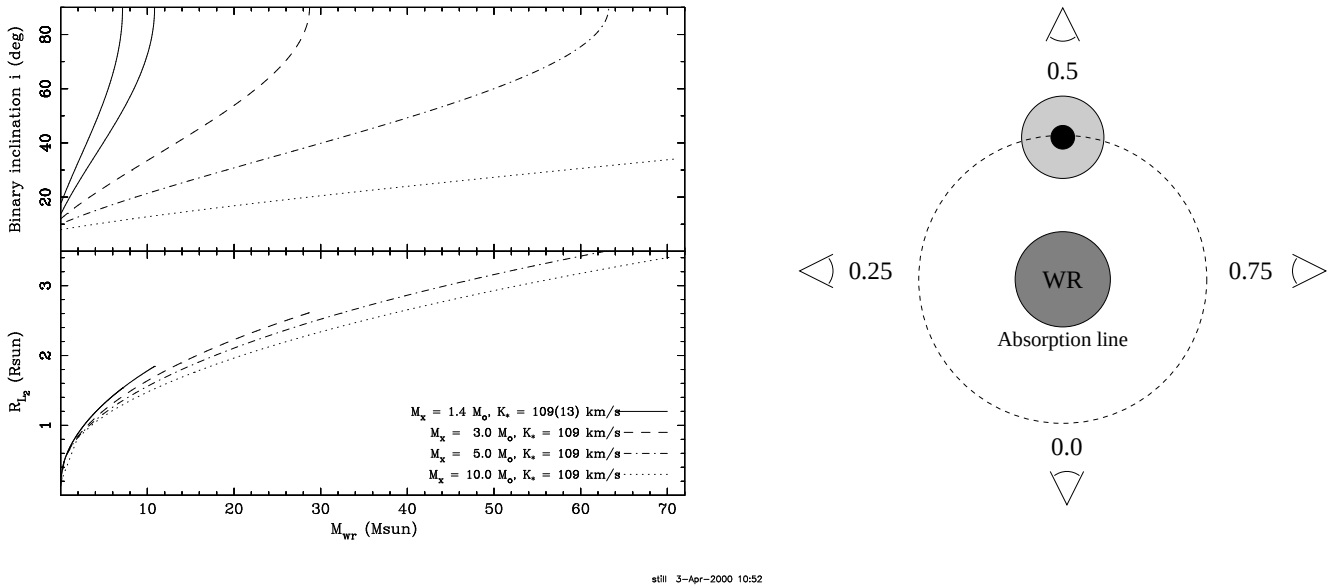

FIG. 10.— Orbital solutions assuming the motion traced in Figure 7 and 8 is centered on or associated with the motion of the mass donor He star. On the left (10a) is shown orbital solutions for differing input mass of the compact object, $M_X = 1.4$ to 10 $M_\odot$, displayed versus inclination and Roche lobe radius. Two solid curves are given for the $M_X = 1.4$ $M_\odot$, solution, which illustrates the plus-minus error range on K. This second set of solutions allows for the high inclination suggested by the X-ray and infrared modulation simultaneously with moderately high mass solutions and Roche lobe radii for the mass donor. The orbital orientation implied by this interpretation is indicated in the panel to the right (10b). It allows for X-ray orbital minimum to occur when the X-ray source is furthest from the observer, at superior conjunction. This configuration gives the most reasonable set of solutions for the orbit of the Cyg X-3 system.

measurement (109 ± 13 km s^{-1}). This orientation, where the absorption is centered on the accretor, is illustrated in Fig 9b. We see from Fig 9a that for all accretor masses, unless the He star is much less massive than implied from luminosity arguments (i.e. $\leq 2M_\odot$), the inclination of the system must be much lower ($\leq 50°$) than is generally accepted based on the X-ray and infrared modulation. Furthermore, any solution that allows for a reasonable inclination, $\geq 50°$, simultaneously gives an absurdly small, nearly non-physical, value for the Roche lobe radius of the donor. As a result we do not consider an origin for the absorption line in the accretion disc or any other material centered on the accretor to be very likely.

Rather, our analysis implies the most likely configuration is the second case, that the material creating the absorption feature is centered on the mass donor. Solutions for this interpretation are presented in Fig 10a and a schematic illustrating the orientation with phase is shown in Fig 10b. Again, two solid curves are given to illustrate the range of solutions consistent with the mass accretor being a neutron star, $M_x = 1.4$ M$_\odot$, given our error on the velocity measurement. In this orientation, X-ray minimum occurs at superior conjunction of the accretor. It is immediately apparent from Fig 10a that realistic high-inclination solutions are now available. Using this interpretation we directly derive the mass function of the system, which is 0.027 M$_\odot$. The reason this does not constrain at all the nature of the accretor is the large, probably dominant, mass of the He donor star. For a neutron star accretor of 1.4 M$_\odot$ the mass of the He star is most likely in the range $5\ M_\odot \lesssim M_{\rm WR} \lesssim 11\ M_\odot$, assuming the system has a moderately high inclination, $i > 60°$.

However, if the accretor is a black hole, there is much less confidence about the mass of the He star. Charles (1998) lists derived masses for black holes in *low-mass* X-ray binaries and finds them to be in the range 5–12 M$_\odot$. Careful inspection of Fig 10a reveals that this allows a wide range of possible solutions, most of which are compatible with very large masses indeed (i.e. several tens of M$_\odot$) for the He star. This is because the Roche radius given in Figure 10a increases for greater He star mass and easily stays within the expected radius limit for such stars (Langer 1989). Moreover, the Roche radius of the He star shown in Figure 10a can even be less than its R$_\star$, as shown in Langer's Figure 5. This is because the tenuous outer atmospheric radius of the star, identified as R$_\star$, contributes an insignificant fraction of the mass of the star, and can extend well beyond the dynamical Roche radius. Nonetheless, we see from Figure 10a that solutions for a $M_{\rm BH} \gtrsim 10$ M$_\odot$ would be inconsistent with our assumption of even a moderate inclination for the binary system, for any realistic companion star mass, $M_{\rm WR} \lesssim 70$ M$_\odot$. For this reason, we put an upper limit on the mass of the compact object of $M_{\rm BH} \lesssim 10$ M$_\odot$. The well known high mass X-ray binary system Cyg X-1 has a similar mass estimate for its black hole (Charles 1998).

We note that in the binary orientation proposed by Schmutz et al. (1996), which lead them to argue for a most likely value of $M_{\rm BH} \approx 17$ M$_\odot$ for the compact object, the absorption feature would be required to arise from a region centered not on the He star or accretor, but a quarter of a cycle out of phase with either orientation.

4.3. *The nature of the stellar companion*

The assumptions used to determine stellar mass in Figure 10a also provide limits for the radius of the stellar companion of Cyg X-3. We are able to test whether this result is consistent with the characteristics, most specifically the luminosity, predicted from atmosphere models and observations of typical WR stars.

The distance to Cyg X-3 is not directly known. However, Dickey (1983) has suggested a lower limit on the distance, $11.6 \times \pi/10$ kpc, where π is the distance in kpc to the galactic center, based on the detection of high velocity neutral hydrogen absorption features and applying a flat rotation curve for the Galaxy. With an updated value for the distance to the Galactic center of ~ 8 kpc (Reid 1993), this gives a lower limit to Cyg X-3 of ~ 9 kpc. Original estimates of the line of sight extinction to Cyg X-3, $A_V = 15$, were made by Becklin et al. (1973). More recent measurements suggest a slightly higher value of $A_V = 19$ (Molnar et al. 1988), $A_J = 5.5$ (van Kerkwijk et al. 1996) which corresponds approximately to $A_V = 19$, and $A_J = 6.0$ (Fender et al. 1996) corresponding to approximately $A_V = 20.5$ (Rieke & Lebofsky 1985). Determining the line of sight extinction is dependent on measuring the flux distribution over a large enough wavelength range to note the differential change, as done by both van Kerkwijk et al. and Fender et al. But equally important, one must simultaneously make assumptions about the functional form of that extinction and the functional form of the underlying continuum of the source. For this reason, without an *a priori* quantitative understanding of the stellar companion, the line of sight extinction cannot be as well constrained as one might hope. Mindful of these limitations, we have used the apparent magnitudes of Cyg X-3 given by Wagner et al. (1989) and Fender et al. (1996), $m_I = 20.0$, $m_H = 13.11$, $m_K = 11.76$ and applied an extinction of approximately $A_V = 20$ and a distance of 9 kpc to obtain absolute magnitudes of $M_I = -4.8$, $M_H = -5.2$, $M_K = -5.1$ for the stellar companion. It is precisely these values, the very luminous lower limits for the absolute magnitude of the stellar companion, that most strongly challenge the notion of Cyg X-3 being a low mass X-ray binary system (Mitra 1998)

We have argued that while in quiescence, the emission lines seen in Cyg X-3, presumably dominated by the companion star, look most similar to the lines seen in early WN-type (WNE) WR stars (FHP99). Based on direct measurements of WNE stars given in Smith et al. (1994), a mass range from 6 to 12 M$_\odot$, corresponds to a typical, $-4 > M_V > -4.8$. Naturally, there is a large scatter in the observed relation. Without a direct determination of M_V, with the uncertainties in the bolometric correction and with the difficulty in extrapolating the extinction characteristics towards Cyg X-3, the luminosity for the stellar component of Cyg X-3 is not highly inconsistent with the luminosity of other WNE stars.

4.4. *The nature of the accretor*

The crucial question of whether the accretor is a neutron star or a black hole cannot be decided with confidence. The only *direct* observational evidence for the presence of a neutron star in Cyg X-3 was in the report of 12.6 ms γ-ray pulsations, ~ 15 years ago (Chadwick et al. 1985).

However, this result has never been widely accepted. As already stated, Schmutz et al. (1996) argue that the observational evidence supports a black hole accretor, which prompted Ergma & Yungelson (1998) to investigate the evolution of such a system. They concluded that Cyg X-3 *may* contain a black hole accreting at super-Eddington rates. Mitra (1998) however argued strongly *against* the interpretation of Schmutz et al. (1996), preferring a low-mass system (which is extremely hard to reconcile with the very high luminosity of the system). For now we will have to consider a fairly large range of accretor masses up to $M_{BH} \lesssim 10\ M_\odot$ (see discussion in §4.2).

5. CONCLUSIONS

The X-ray binary, Cyg X-3, is the only known system containing a (presumably) massive He star with a compact object. This makes Cyg X-3 a uniquely important link in our understanding and testing of massive X-ray binary evolution. In this paper we pursued an emission line analysis of the quiescent and outburst spectra presented in FHP99. We reported that while the double-peaked emission seen in the He I lines during outburst are consistent with a disk-wind geometry as proposed in FHP99, our tomographic analysis in particular reveals unresolvable ambiguities in the mechanism responsible for the formation of double-peaked emission. For this reason, additional constraining spectral information or methods are needed to resolve the nature of the double-peaked emission and its relation to the wind or disk geometry of the system during outburst.

Of greater significance was the detection of a weak absorption feature threading through the blue wing of the 2.0587 μm He I line. This feature moves $\sim 1/4$ out of phase with all other spectral modulations seen in Cyg X-3, consistent with He I absorption originating in an isotropic, asymptotic wind from the companion star. Consequently it can be used to derive the first radial velocity curve for the Cyg X-3 system. Employing reasonable geometric assumptions, we derive a mass range of $5\ M_\odot \lesssim M_{WR} \lesssim 11\ M_\odot$ for the He star, if the accretor is a neutron star. Additionally, should the accretor be a black hole, we determine $M_{BH} \lesssim 10\ M_\odot$, based on an upper mass limit, $M \lesssim 70\ M_\odot$, for the He star companion.

Identification of the critical absorption feature used in obtaining a mass function for the Cyg X-3 system was made possible only through phased-resolved near-infrared observations. A further key was obtaining observations during outburst. Clearly, periods of high X-ray variability would make the most opportune times to catch this rare infrared state once more. The spectra presented in FHP99 represent the best quality a 4-meter class telescope will likely ever deliver on this object, and yet these spectra barely detect the very weak, sometimes very broad, and often heavily blended features. Its not certain that moving to an 8-meter class telescope would resolve all the problems with the current data set, as many of the lines are already resolved with the current spectra. However, the narrow absorption feature detected in the outburst spectrum may be just the first of many similarly weak and narrow features which might better be revealed with higher-quality spectra. Such features offer promise in resolving the ambiguities plaguing our analysis.

FHP99 showed there to be a marked decrease in X-ray flux during the four days prior to the near-infrared outburst, the minimum occurring just after outburst. This may have resulted from drops in the ionization state of the wind following a temporary decrease in the X-ray flux. FHP99 showed that the outburst occurring in June 1997 and previous outbursts suggested in earlier spectra (van Kerkwijk et al. 1996) were short lived ($\leq$ 24-h). Careful day-to-day monitoring of Cyg X-3 in the X-ray and radio, particularly during epochs of high X-ray and radio activity, would potentially precede suitable windows for near-infrared spectroscopic observations of P Cygni lines.

We are grateful for comments made by our referee which lead us to greatly improve the presentation of this work. Observations reported in this paper were obtained with the Multiple Mirror Telescope, operated by the Smithsonian Astrophysical Observatory and the University of Arizona. We are grateful to G. and M. Rieke for their critical support in this program. M. M. H. received support for this work provided by The University of Cincinnati through a University Research Council Grant and a Faculty Summer Fellowship.

REFERENCES

Becklin E.E., Neugebauer G., Hawkins F.J., Mason K.O., Sanford P.W., Mathews K., Wynn-Williams C.G., 1973, Nature, 245, 302
Burrows, A., Woosley, S.E. 1986, ApJ, 308, 680
Dickey, J.M., 1983, ApJ, 273, L71
Chadwick P. M. Dipper N. A., Dowthwaite J. C., Gibson A. I., Harrison A. B., 1985, Nature, 318, 642
Charles, P.A. 1998, *Black Holes in our Galaxy : observations*, In : Abramowicz, M. A., Björnsson, G., Pringle, J. E. (Eds), Theory of Black Hole Accretion Discs, Cambridge Contemporary Astrophysics, CUP, 1998, p.1
Conti, P. 1996, in *Wolf-Rayet stars in the framework of stellar evolution*, Ed. J.M. Vreux, A. Detal, D. Fraipont-Caro, E. Gosset, and G. Rauw (Liege: Universite de Liege, Institut d'Astrophysique) p.655
Ergma E., Yungelson L.R., 1998, A&A, 333, 151
Fender R.P., Bell Burnell S.J., Williams P.M., Webster A.S., 1996, MNRAS, 283, 798
Fender, R.P., Hanson, M.M., & Pooley, G.G. 1999, MNRAS, 308, 473 (FHP99)
Hulse, R.A., Taylor, J.H. 1975, ApJL, 195, 51
Kitamoto, S. et al., 1995, PASJ, 47, 233
Langer, N. 1989, A&A, 210, 93
Lépine, S., Moffet, A.F.J. 1999, ApJ, 514, 909
Marsh, T. R., Horne, K., 1988, MNRAS, 235, 269
Mason K.O., Cordova F.A., White N.E., 1986, ApJ, 309, 700
Mitra A., 1996, MNRAS, 280, 953
Mitra A., 1998, ApJ, 499, 385
Molnar, L.A., Reid, M.J., Grindlay, J.E., Willner, S.P., 1988, BAAS, 20, 736
Morris, P.W., Eenens, P.R.J., Hanson, M.M., Conti, P.S., Blum, R.D. 1996, ApJ, 470, 597
Paerels, F., Cottam, J., Sako, M., Liedahl, D.A., Brinkman, A.C., van der Meer, R.L.J., Kaastra, J.S., Predehl, P. 2000, ApJ Letters, in press
Parsignault D.R. et al., 1972, Nat. Phys. Sci. 239, 130
Reid, M. J. 1993, ARA&A, 31, 345
Rieke, G.H. & Lebofsky, M.J. 1985, ApJ, 288, 618
Sanford P.W., Hawkins F.H., 1972, Nat. Phys. Sci. 239, 135
Schalinski C.J. et al., 1998, A&A, 329, 504
Schmutz W., Geballe T.R., Schild H., 1996, A&A, 311, L25
Skilling, J., Bryan, R. K., 1984, MNRAS, 211, 111
Smith, L.F. 1968, MNRAS, 138, 109
Smith, L.F., Meynet, G., & Mermilliod, J.-C. 1994, A&A, 287, 835
van den Heuvel, E., P., J., & De Loore, C. 1973, A&A, 25, 387

van Kerkwijk, M.H. et al., 1992, Nature, 355, 703
van Kerkwijk M.H., Geballe T.R., King D.L., van der Klis M., van Paradijs J., 1996, A&A, 314, 521
Wagner, R.M., Kreidl, T.J., Bus, S.J., Williams, W., 1989, ApJ, 346, 971
Willams, D., Thompson, C.L., Rieke G.H., Montgomery, E. 1993, Proc. SPIE 1308, 482.
Williams, P.M. & Eenens, P. 1989, MNRAS, 240, 445